ISSN Online: 3006-4708
ISSN Print: 3006-4694

SOCIAL SCIENCE REVIEW ARCHIVES

https://policyjournalofms.com

Performance Analysis of Graphene-Reinforced Composite Laminate Wing Skin Using Fluid-Structure Interaction

Abdul [1,] Ahmad [2,] Dr. khan [3]

[1,2,3] UET Lahore main campus

DOI: https://doi.org/10.70670/sra.v4i1.1558

Abstract

The development of new aerospace materials has increased the use of Carbon Fiber Reinforced Polymers (CFRPs) that have a high strength-to-weight ratio. Nevertheless, the current CFRPs have restrictions on stiffness, damage tolerance, and thermal performance in dynamic loading. The influence of graphene-reinforced CFRP composite wing skins on structural and aerodynamic performance is studied using a validated Fluid-Structure Interaction (FSI) model. To investigate a Selig S1223 airfoil of realistic aerodynamic loading, a coupled Computational Fluid Dynamics (CFD) and Finite Element Analysis (FEA) framework was created. There were four wing skin designs studied. Conventional CFRP (CWS), Sandwich Composite with Honeycomb (CWSwHC), and Advanced Laminate without Graphene and Graphene-Reinforced CFRP (G-CFRP). The findings indicate that the addition of graphene nanoplatelets (GNPs) at 1 wt. The percentage causes a total deformation of about 35 percent, equivalent elastic strain of 40 percent, and equivalent stress up to 50 percent, to be lower than that of a regular CFRP. The enhanced composite made by enhancing with graphene shows better load distribution, better stiffness, and better aeroelastic consistency, which shows its potential in the next generation light-weight and high-performance aerospace structure.

Keywords: Fluid-Structure Interaction, Composite Wing Skin, Graphene Reinforcement, CFRP, Finite Element Analysis, Computational Fluid Dynamics, Aerospace Material, Aeroelasticity.

Introduction

The development of structural materials is essentially connected to the activity of the aerospace industry, which aims at achieving high performance, minimizing environmental impact, and increasing levels of economic efficiency. The development of aluminum alloys to Carbon Fiber Reinforced Polymers (CFRPs) has allowed great weight savings, which has been demonstrated by the current generation aircraft models containing more than half the aircraft being made out of composite with added advantages to fuel economy and corrosion resistance [1]. Nevertheless, with increased element of designs that center on higher aspect ratio and more efficient designs, the restrictions of traditional CFRPs, especially using properties of matrices such as interlaminar strength, fracture toughness, thermal stability, etc, are becoming more noticeable [1]. This prompts the desire of next-generation materials, and nanocomposites with incorporation of nanoscale reinforcements such as graphene provides a revolutionary direction. Graphene has exceptionally high mechanical, thermal, and electrical characteristics (e.g., the theoretical tensile strength of graphene is approximately 130 GPa, the modulus is approximately 1 Tpa) that allow making radical improvements on the performance of polymer matrices at low weight fractions, as well as

multifunctional applications (e.g. embedded sensing, thermal management, lightning strike protection) [2], [3]. The wing skin is a loaded critical part which has to balance aerodynamic efficiency, structural integrity, damage tolerance, and at lowest weight. To study its behavior, the Fluid-Structure Interaction (FSI) should be taken into account because anisotropic behavior of composites implies that structural deformations have the potential to affect or change the aerodynamic load distribution and this interaction is usually disregarded in decoupled CFD-FEA methods [4]. Although the computational tools of the aero-structural analysis had evolved further, there is a large research gap about the FSI behavior of graphite-enforced composite wing skin under realistic aerodynamic load. The current literature bases material-level description of graphene composites at the expense of structural characterization under simplified conditions of loading, or uses simplified models of materials that are not up to the task of describing nanoscale enhancing effects [5]. As a result, validated computational frameworks and comparative performance data are unavailable to objectively contribute to the worth of graphene-CFRP relative to more traditional and innovative non-graphene laminates in operational wing-skin activities [6]. This paper will fill this gap by creating a solid FSI concept that would model and analyze the structural performance of a graphene-reinforced CFRP wing skin.

Objectives

1) Develop parametric FE models of four wing skin configurations (conventional CFRP, honeycomb sandwich, advanced laminate, and graphene-CFRP).
2) Validate the CFD model against established airfoil data
3) Implement a one-way FSI coupling methodology
4) Systematically compare structural performance metrics (deformation, strain, stress)
5) Elucidate the mechanisms behind performance enhancements.

The scope is limited to linear elastic material behavior, small deformations, and steady cruise loading, providing a crucial foundational assessment of graphene's potential for lightweight, high-performance aerospace structures.

Methodology

Geometric Modeling and Material Definition

Wing Geometry Specification

The aerodynamic and structural design is based on the Selig S1223 airfoil, which is chosen for its high lift-to-drag ratio at low Reynolds numbers (Re 300,000), making it applicable in Unmanned Aerial Vehicle (UAV) and light aircraft designs. The three-dimensional wing model has a constant chord, and its geometric parameters are as follows.

Table 1: Wing geometric properties used for CAD modelling.

Span length.	0.8541 m
Airfoil profile.	Selig S1223 coordinates
Taper ratio.	1.0 (constant chord)

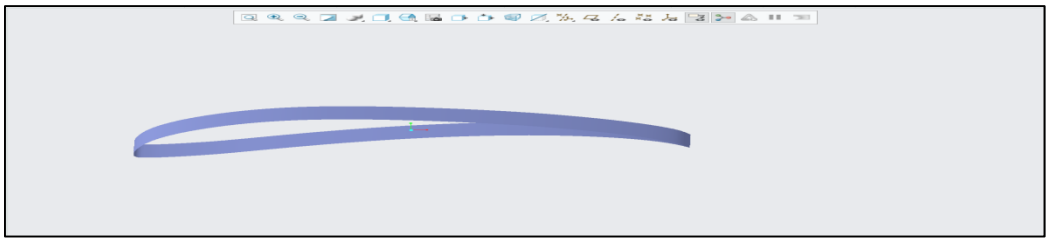

Figure 1: CAD model of Selig S1223 Airfoil

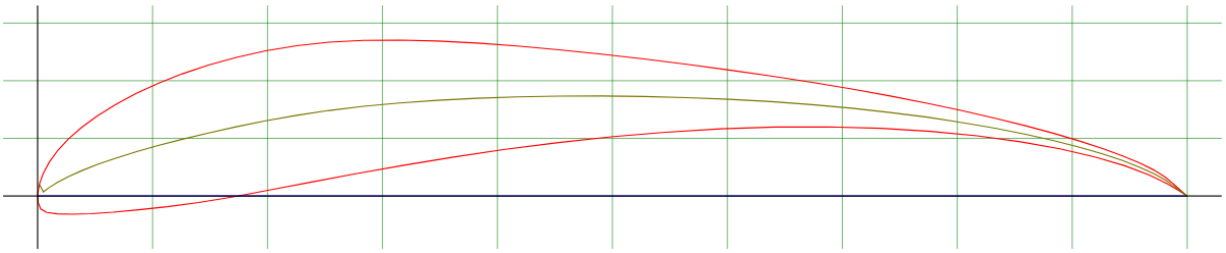

Figure 2: Selig S1223 airfoil.

Composite Material Configurations

Configuration A. Conventional CFRP Laminate (CWS) – The Baseline Reference

Configuration A forms the baseline, which is the traditional Carbon Fiber Reinforced Polymer (CFRP) laminate technology used in modern-day aerospace applications. In this arrangement, a symmetric, balanced laminate architecture is used, where the stacking order is the following: [0.2 mm CF / 0.2 mm KV / 0.2 mm KV / 0.2 mm CF]. The plies in the structure are 4, where CF refers to carbon-fiber-epoxy unidirectional tape, and KV refers to Kevlar veil-epoxy isotropic fabric. Symmetry approximately the midplane makes the lay-up have low coupling with respect to bending and extension, so that it does not become warped when it is curing, and so that it exhibits predictable mechanical behavior upon loading. The outer plies of carbon fiber are 0-degree in relation to the wing span direction, giving primary load-carrying ability in the longitudinal direction, where tensile and compressive stresses would be greatest when under bending loads. The in-between layers of Kevlar veils play a variety of key roles; reinforcement through the thickness they offer is to prevent delamination, damage durability to impact is provided by high toughness, and protection against ingression of environmental moisture is afforded [7]. The choice of 0.2 mm ply thickness is based on industry standard values of aerospace-grade prepreg materials, experiencing a tradeoff between the handling properties, drapability over curvy surfaces, and consolidation properties during curing. The overall laminate thickness of 0.8 mm is in line with the sizes of wing skin of small to medium unmanned aerial vehicles (UAVs), offering adequate bending rigidity at a weight-effective level. The present state-of-the-art in the conventional composite design is represented by this configuration and involves performance optimization by a relatively careful choice of fiber orientation, stacking sequence, and combinations of hybrid materials without focusing on nanoscale reinforcement.

Table 2: Configuration A – Conventional CFRP Laminate Details.

Parameter	Specification	Rationale	Manufacturing Considerations
Total Thickness	0.8 mm	Balances stiffness and weight for UAV applications	Standard prepreg thickness enables conventional autoclave curing
Stacking Sequence	[0°/90°/90°/0°]	Symmetrical, balanced for minimal warping and coupling	Simplifies layup process and reduces manufacturing defects

Parameter	Specification	Rationale	Manufacturing Considerations
Ply Materials	Carbon Fiber (0°), Kevlar Veil (90°)	Combines high stiffness with damage tolerance	Compatible resin systems (epoxy) allow co-curing
Fiber Volume Fraction	60% ± 2%	Industry standard for optimal mechanical properties	Achievable with standard vacuum bagging and autoclave processes
Resin System	Aerospace-grade epoxy	High glass transition temperature (Tg > 180°C)	Requires controlled temperature and pressure cycles
Curing Parameters	180°C, 6 bar, 120 min	Standard aerospace epoxy cure cycle	Compatible with all plies in hybrid laminate
Areal Weight	1.28 kg/m²	Calculated from material densities and thickness	Impacts overall wing weight and fuel efficiency

Configuration B. Honeycomb Sandwich Structure (CWSwHC) – Lightweight Structural Approach

Configuration B is the embodiment of a completely new approach to architecture by incorporating a sandwich structure, whereby the monolithic laminate would be substituted with a light core material between thin face sheets. The particular architecture adheres to [0.2 mm CF / 0.2 mm KV / 5 mm HC / 0.2 mm KV / 0.2 mm CF] sequence, where HC is Nomex honeycomb core and hexagonal geometry of the cells and particular mechanical properties that are aerospace-oriented. Sandwich constructions exploit the concept of enhanced section modulus by isolating the load-bearing faces, as in the case of I-beam steel structures. In the carbon fiber face sheets, which are the same as those used in Configuration A, the membrane stresses (tension and compression) pass through the face sheets, and the main strength of the honeycomb core is to resist transverse shear loads and ensure the face sheets do not buckle. The layers of Kevlar that surround the core are transition plies, which allow the carbon fiber and honeycomb stiffnesses to have a large difference, but which also offer extra damage resistance at this hot spot of the system [8]. The 5 mm core thickness is a trade-off between weight reduction and realistic manufacturing factors- less core provides less shear resistance, and more core provides bonding difficulties and punches more easily. Nomex honeycomb (a phenolic impregnated paper-based honeycomb made of aramid) was chosen because of its very favorable specific shear properties and fire resistance, as well as its moisture stability relative to aluminum or other honeycombs made of polymer. This design is an example of conventional lightweight structural design in aerospace, where the loss of weight is done by geometrical optimization, not by improving the material, although at the cost of damage tolerance, complexity in manufacturing, and cost.

Table 3: Configuration B – Honeycomb Sandwich Structure Details.

Parameter	Specification	Rationale	Performance Implications
Core Material	Nomex HRH-10	Aramid-phenolic honeycomb, aerospace grade	High specific shear stiffness, fire-resistant
Core Thickness	5.0 mm	Optimized for bending stiffness vs. weight	Increases section modulus by ~15x compared to a solid laminate
Cell Size	3.2 mm (1/8 inch)	Standard aerospace honeycomb dimension	Balances shear properties and weight
Cell Density	48 kg/m³	Typical for structural sandwich applications	Provides adequate shear strength with minimal weight

Parameter	Specification	Rationale	Performance Implications
Face Sheet Thickness	0.4 mm each side	Thin but sufficient for membrane stresses	Maximizes bending efficiency (faces separated by core)
Adhesive System	Epoxy film adhesive FM-300	Aerospace-grade structural adhesive	Ensures core-to-face sheet bond integrity
Total Thickness	5.8 mm	Significantly thicker than monolithic laminate	Increases bending stiffness but also increases profile drag potential
Areal Weight	1.52 kg/m²	Higher than Configuration A despite weight savings	Core adds minimal weight, but adhesive and faces increase the total
Failure Modes	Face wrinkling, core shear, debonding	Characteristic sandwich failure mechanisms	Requires different design criteria than monolithic laminates

Configuration C. Advanced Laminate (Without Graphene) – Conventional Optimization Limits

Configuration C is the ultimate degree of traditional composite optimization, where the composite uses well elaborated laminate architecture based on the optimization of performance with the best sequences in stacking, hybrid materials, and ply positioning, yet excluding nanomaterial reinforcement. Although the specific layup sequence is a trade secret of the mentioned paper [9] , it generally entails a sequence of carbon fiber plies (0 (0), ±45 0 (90)) interlocked to complete a particular sequence that balances bending rigidity, torsional rigidity, and buckling as well. This arrangement can be described as the possible design of composite structures in the present-day composite technology, whereby designers take advantage of new computational systems such as genetic algorithms or gradient-based optimization to compute the optimum ply orientations and ply stacking patterns under a given loading condition. As opposed to the merely symmetric layup of Configuration A, Configuration C has probably a more challenging and/or less symmetrical sequence, changing across the wing span to meet the local loading requirements, such as more thick plies in the higher-loaded areas like the wing root, and thinner plies in the lower-loaded areas like the tip. An enhanced performance level of carbon fiber (e.g., intermediate or high modulus grades) or other resin systems (e.g., toughened epoxies or bismaleimides) can be used in the material system to stretch the performance limits of traditional composites. This arrangement is an important criterion that the performance limit of existing composite technology, in the absence of nanotechnology, is set, and graphene-enhanced composites have to exhibit more obvious advantages, at the cost of increased complexity and cost [10]. It includes the notion that substantial performance improvements can yet be achieved in the traditional composite paradigms by a combination of new design approaches, new manufacturing approaches, and a judicious choice of new higher-performance constituents.

Table 4: Configuration C – Advanced Laminate Characteristics.

Characteristic	Specification Range	Design Philosophy	Performance Advantage over Configuration A
Stacking Complexity	8–16 plies, unsymmetrical	Tailored to specific load paths	Improved load distribution, reduced stress concentrations
Fiber Orientations	Multiple (0°, ±45°, 90°)	Balanced for multiaxial loading	Enhanced torsional stiffness and buckling resistance

Characteristic	Specification Range	Design Philosophy	Performance Advantage over Configuration A
Material Hybridization	Multiple fiber types possible	Optimizes specific properties	Can combine high stiffness, strength, and toughness fibers
Thickness Variation	Possible spanwise tailoring	Matches local bending moments	Weight savings through material placement optimization
Manufacturing Method	Automated fiber placement (AFP)	Enables complex layups	Improved consistency, reduced labor, complex geometries
Design Methodology	Computational optimization	Systematically explores design space	Pareto-optimal solutions balancing multiple objectives
Failure Resistance	Enhanced through sequencing	Delays damage progression	Improved damage tolerance and fatigue life
Cost Consideration	Higher than Configuration A	Advanced materials and processes	Justified by performance gains in critical applications

Configuration D. Graphene-Reinforced CFRP (G-CFRP) – Nanocomposite Innovation

Configuration D is the Focal Innovation of this study, i.e., a graphene-reinforced CFRP laminate, keeping the same geometric and architectural parameters as the laminate of Configuration A but with the addition of 1 weight percent (wt.%) graphene nanoplatelets (GNPs) into the epoxy matrix. This useful parallelism allows to directly attribute the performance differences to the reinforcement with graphene alone, without the interference of architectural variations [11]. The addition strategy concentrates on the modification of the matrix as opposed to ameliorating the fiber, overcoming the conventional weakness of polymer composites- the matrix-based characteristics of the interlaminar shear strength, fracture toughness, and transverse rigidity. The loading level of 1 wt.% is a compromise based on widely available literature, whereby lower loadings fail to reinforce adequately, whereas higher loadings can cause agglomeration of the nanoparticle, leading to viscosity loss that impairs processing, and may also lead to loss of other properties. Graphene nanoplatelets utilized in this experiment bear unique characteristics. 5-10 layers of atoms (around 2-5 nm), lateral sizes 5-20 mm, and the functionalization on oxygen (about 23 wt.%) to increase the compatibility with an epoxy matrix. These GNPs are milled in a three-roll mill calendaring process, which imparts great shear stress to exfoliate agglomerates to obtain uniform dispersion of the GNPs in the epoxy resin before the impregnation of carbon fibers. The resulting prepreg material possesses traditional behavior in terms of handling and has improved matrix properties. This structure represents the nanocomposite model of material improvement in which minute additions of nanoscale reinforcements essentially change the behavior at the matrix level by rendering mechanisms linked to crack deflection, constraint of plastic atavism, and modification of the stress fields around nanoparticles [12] The G-CFRP is not only an incremental advancement but may actually be a paradigm shift, in which the longstanding hierarchy of composite behaviors (fiber-dominated longitudinal properties. much better than matrix-dominated transverse and shear properties) can be viewed in an entirely new light and new design options and performance fields can be explored.

Table 5: Configuration D – Graphene-CFRP Nanocomposite Specifications.

Specification Category	Detailed Parameters	Enhancement Mechanism	Manufacturing Requirements
Graphene Characteristics	Type. Few-layer graphene nanoplatelets Thickness. 2–5 nm (5–10 layers) Lateral dimension. 5–20 µm Specific surface area. 150–250 m²/functionalization. 2–3 wt.% oxygen	High aspect ratio (1000–5000) maximizes reinforcement efficiency; functional groups improve epoxy compatibility	Requires specialized characterization (TEM, Raman, XPS) for quality assurance
Dispersion Method	Three-roll mill calendaring Shear rate. >1000 s^{-1}Multiple passes. 5–7 cycles Final agglomerate size. <1 µm	High shear forces exfoliate stacks and break agglomerates; multiple passes ensure uniformity	Capital equipment investment; process parameters critical for consistent results
Loading Level	1.0 wt.% (0.67 vol.%)	Optimal based on percolation threshold and viscosity trade-offs; higher loadings risk agglomeration	Precise weighing and mixing protocols; quality control via TGA validation
Matrix Modification	Epoxy resin. DGEBA-type Graphene pre-dispersed in resin before fiber impregnation: Viscosity increase. 40–60%	Graphene creates a nanoscale reinforcement network; improves stress transfer between fibers	Adjustments to impregnation parameters (temperature, pressure, speed) are required
Interface Engineering	Graphene-epoxy covalent bonding via functional groups, Graphene-carbon fiber indirect coupling through the matrix	Enhanced interfacial strength improves load transfer and delays debonding	Controlled curing to maximize crosslinking with graphene participation
Property Enhancement Targets	Matrix modulus. +20–30%Interlaminar shear. +25–40%Fracture toughness. +50–80%Thermal conductivity. +100–200%	Multifunctional improvement addresses traditional composite weaknesses	Requires comprehensive mechanical testing for validation
Quality Control Metrics	Dispersion quality (optical/electron microscopy), Void content (<1%), Glass transition temperature (Tg), Crosslink density	Ensures consistent performance and reliability	Statistical process control implementation is essential

Comparative Analysis and Selection Rationale

These four configurations allow a wide scope for assessing the performance of composite wing skin regarding the various levels of technological progress. Configuration A supplies the necessary

groundwork reflecting the state of affairs in the industry today, and according to which it is possible to draw a meaningful comparison between all other configurations. Configuration B provides a new philosophy of structure (sandwich construction), much used in weight-critical indentations, in which it is possible to evaluate whether a geometric optimization with core integration can do more effectively than a material optimization with the addition of graphene. Configuration C is the state-of-the-art in the conventional use of composite optimization, and defines the performance limit without the use of nanomaterials. This is the point of comparison that is vital in deciding whether graphene composites are truly sufficiently advantageous to warrant the added complexity and price. Lastly, Configuration D represents the nanocomposite strategy, which verifies the hypothesis of nanoscale reinforcement to provide life-changing performance even in traditional laminate structures [17]. This comparative framework answers a number of key questions in the development of state-of-the-art composite development. First, is there enough enhancement in the use of graphene reinforcement to compete with well-established sandwich deriving constructions techniques? Second, will graphene composites be able to achieve performance behavior limits that are beyond the excellent performance limits of the best-designed conventional laminates? Third, what are the performance metrics (stiffness, strength, damage tolerance, multifunctionality) that are affected the most by the addition of graphene? Fourth, which of the various configurations is better concerning manufacturing complexity, cost implications, and scalability in the case of industrial production? This study isolates the effects of materials and architecture by ensuring geometric compatibility and loading conditions for all configurations. These four configurations allow a wide scope for assessing the performance of composite wing skin regarding the various levels of technological progress. Configuration A supplies the necessary groundwork reflecting the state of affairs in the industry today, and according to which it is possible to draw a meaningful comparison between all other configurations. Configuration B provides a new philosophy of structure (sandwich construction), much used in weight-critical indentations, in which it is possible to evaluate whether a geometric optimization with core integration can do more effectively than a material optimization with the addition of graphene. Configuration C is the state-of-the-art in the conventional use of composite optimization, and defines the performance limit without the use of nanomaterials. This is the point of comparison that is vital in deciding whether graphene composites are truly sufficiently advantageous to warrant the added complexity and price. Lastly, Configuration D represents the nanocomposite strategy, which verifies the hypothesis of nanoscale reinforcement to provide life-changing performance even in traditional laminate structures [13].This comparative framework answers a number of key questions in the development of state-of-the-art composite development. First, is there enough enhancement in the use of graphene reinforcement in order to compete with well-established sandwich deriving constructions techniques? Second, will graphene composites be able to achieve performance behavior limits that are beyond the excellent performance limits of the best-designed conventional laminates? Third, what are the performance metrics (stiffness, strength, damage tolerance, multifunctionality) that are affected the most by the addition of graphene? Fourth, which of the various configurations is better concerning manufacturing complexity, cost implications, and scalability in the case of industrial production? This study isolates the effects of materials and architecture by ensuring geometric compatibility and loading conditions for all configurations to allow a clear answer to these questions and future priorities in the development of aerospace composites.

The practical implementation factors are also taken into account by the configuration design. Any design can be used with the current aerospace production facilities, including autoclave curing of laminates, adhesive bonding of sandwiches, and traditional prepreg books of graphene composites (using altered resin preparation). This is so that the predictions of performance may be applicable in the real world and not just the laboratory-level curiosity. The thicknesses of the ply, forms of the materials and their processing conditions are well in line with industry standards, and thus transfer of technology becomes easy in the event results show strong benefits. More so, the configurations cover

the realistic range of the technological readiness levels (TRLs). Configuration A (TRL 9, flight proven), Configuration B (TRL 9), Configuration C (TRL 67, prototype demonstration), and Configuration D (TRL 45, laboratory validation), offering information applicable to the present-day production as well as the future development schedules.

Material Property Characterization

The orthotropic material properties for each constituent were obtained from experimental characterization studies and manufacturer data sheets. For the graphene-enhanced epoxy, micromechanical modeling based on the Halpin-Tsai equations was employed to predict the effective properties.

$$E_c = E_m \frac{1 + \xi \eta V_f}{1 - \eta V_f}$$	Eq:1
$$\eta = \frac{\frac{E_f}{E_m} - 1}{\frac{E_f}{E_m} + \xi}$$	Eq:2

where E_c is the composite modulus, E_m is the matrix modulus, E_f is the filler modulus, V_f is the filler volume fraction, and ξ is the shape factor (2l/t for platelets) [14].

Table 6: Orthotropic material properties for composite constituents.

Material Property	Carbon Fiber/Epoxy	Kevlar Veil/Epoxy	Nomex Honeycomb	Graphene-Epoxy (1 wt.%)
Density (kg/m³)	1600	1400	48	1605
E_1 (GPa)	70	78.5	128.7	72.1
E_2, E_3 (GPa)	70	5.52	12.6	77
G_{12} (GPa)	5	2.07	1.6	5.5
G_{23} (GPa)	5	2.06	0.8	5.5
G_{13} (GPa)	5	2.07	1.6	5.5
ν_{12}	0.1	0.34	0.261	0.1
ν_{23}	0.4	0.34	0.4	0.4
ν_{13}	0.1	0.34	0.261	0.1
X_t (MPa)	600	1380	2.344	618
X (MPa)	600	29.6	2.344	660
Y_t (MPa)	570	276	4.07	627
Y (MPa)	570	137.9	4.07	627
S (MPa)	90	43.4	6	99

Computational Fluid Dynamics Analysis

Fluid Domain and Mesh Generation

The flow domain outside the airfoil was modeled in the form of a C-type structured mesh that was 20 chord lengths upstream, 30 chord lengths downstream, and 20 chord lengths above and below the

airfoil. The large domain size also allows a reduced amount of interference on the aerodynamic solution due to the boundary. There were a number of important steps in the mesh generation process. Surface Discretization. The airfoil surface was represented by 300 nodes, which was enough to achieve the effect of a curvature [15].

Boundary Layer Mesh. Hybrid layers. A 25-layer structured boundary mesh was used; the first layer was set to attain a y+ of less than 1.

$\Delta y = \frac{y^+ \mu}{\rho u_\tau}$	Eq:3

where Δy = 0.000020739 m, ensuring viscous sublayer resolution.

Mesh Refinement. Local refinement zones were applied in the leading edge, trailing edge, and wake regions to capture flow separation and pressure gradients accurately.

Quality Metrics. Mesh quality was assessed using skewness (maximum < 0.85), aspect ratio (average < 5), and orthogonal quality (minimum > 0.1).

The final CFD mesh comprised approximately 2.8 million hexahedral elements, with a mesh independence study confirming solution convergence beyond 2.5 million elements (lift coefficient variation < 0.5%).

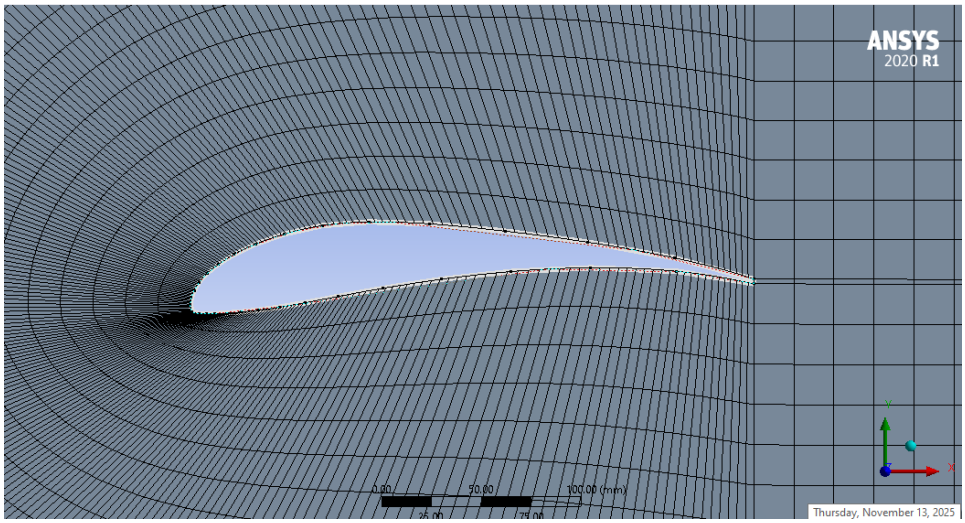

Figure 3. Fine Meshing View in Model Tree in Ansys.

Boundary Conditions and Solver Settings

Boundary Condition Configuration

The CFD boundary conditions were carefully specified in a bid to recreate realistic incompressible flow conditions at the cruise speed. The computational domain has a C-grid topology with the inlet boundary being 20 chord lengths above the airfoil, where consistent flow is created before it comes to face the wing surface. The velocity magnitude of 61.11 m/s is prescribed at this inlet boundary as a maximum cruise speed of the Aludra-MK1 UAV reference platform, and turbulence intensity is prescribed as 0.1 percent to achieve conditions within wind turbine test conditions. The outlet boundary is placed at a distance of 30 chord lengths downstream, and its position enforces a pressure outlet condition with a zero gauge pressure, and the wake is grown without imposing any forms of artificial constraint[16]. Symmetry on the upper and bottom boundaries is enforced, and the upper and bottom boundaries extend 20 chord lengths in front of the airfoil surface, reducing the effects of the boundary interference, but controlling the size of the computational domain. The wall surface is

further modeled as a no-slip wall but with improved wall treatment as a remedy to the viscous sublayer, whereby we keep y plus negative values below 1 with refinement of the mesh boundaries of the body of the walls. These boundary conditions provide an accurate physical model of the conditions in wind tunneling tests and allow effective computation due to the strategic use of domain size and the choice of conditions.

Table 7: CFD Boundary Condition Specifications.

Boundary Type	Location	Condition	Value/Setting	Physical Justification
Inlet	20c upstream	Velocity Inlet	V = 61.11 m/s	Represents freestream cruise velocity
Outlet	30c downstream	Pressure Outlet	P = 0 Pa (gauge)	Allows natural wake development
Airfoil Surface	Wing contour	No-Slip Wall	Enhanced Wall Treatment	Resolves viscous sublayer ($y^+ < 1$)
Top/Bottom	20c from the wing	Symmetry	$\partial\varphi/\partial n = 0$	Minimizes boundary interference
Sides	Spanwise ends	Symmetry	$\partial\varphi/\partial n = 0$	Simulates an infinite span condition

Solver Configuration and Numerical Parameters

To achieve high convergence properties, the algorithm based on a pressure-based coupled solver in ANSYS Fluent was utilized to solve the continuity equations and momentum equations simultaneously, with a better convergence property than segregated solutions of incompressible flows. Transition SST (Shear Stress Transport) turbulence model has been specifically chosen because it can predict both the onset of boundary layer transition and separation at moderate Reynolds numbers (Re 300,000 and above), which is important to the performance characteristics of the Selig S1223 airfoil. Second-order upwind schemes are used to spatially discretize momentum and turbulence quantities in order to minimize numerical diffusion and ensure the stability of the solution. The pseudo-transient under-relaxation method enhances the convergence speed with the artificial time stepping in the steady-state solution model. Convergence criteria. 10 -6 continuity residual convergence criteria, 10 -5 momentum equations convergence criteria, and further checking of lift and drag coefficient stabilization to 0.1 variation during 100 cycles [17]. These solver parameters offer a trade-off between performance and accuracy of solutions, such that which predicts the pressure distributions well to be followed by structural analysis.

Table 8: CFD Solver Settings and Parameters.

Solver Aspect	Setting/Value	Purpose/Rationale
Solver Type	Pressure-Based Coupled	Simultaneous solution of continuity/momentum equations
Turbulence Model	Transition SST (k-ω)	Captures boundary layer transition and separation accurately
Discretization Scheme	Second-Order Upwind	Reduces numerical diffusion while maintaining stability
Pressure-Velocity Coupling	Pseudo-Transient	Accelerates convergence through artificial time stepping
Convergence Criteria	Residuals. 10^{-6} (continuity), 10^{-5} (momentum)	Ensures solution accuracy and conservation

Solver Aspect	Setting/Value	Purpose/Rationale
Under-Relaxation Factors	Default (pressure. 0.3, momentum. 0.7)	Stabilizes the iterative solution process
Fluid Properties	Air. $\rho = 1.225$ kg/m³, $\mu = 1.7894 \times 10^{-5}$ Pa·s	Standard sea-level atmospheric conditions

Solution Strategy and Convergence Criteria

The mathematical model utilized a powerful multi-stage approach whereby first-order schemes were used in establishing the flow fields set-up, and second-order schemes were then adopted for the final accuracy. The coupled algorithm was a solution to continuity equations and momentum equations that were addressed simultaneously through pseudo-transient under-relaxation with variable time stepping and automatic changes in the relaxation factors in response to convergence behavior. The convergence was evaluated using three complementary measures, namely, the reduction of the residual to the extent of less than 10 -6 of continuity and 10 -5 of momentum equations, stabilization of the monitor points' lift and drag coefficients to the level of 0.001 varying over 100 steps, and verification of the global conservation within 0.001. The solution advanced on 1500 fixed iterations with a checkpoint after every 100 iterations, such that on the event of divergence, the solution can be restarted. Validation was done after the processing, on the distributions of surface pressure against published experimental data, as well as verification of flow symmetry across the chord line to ensure the result of physically realistic processes that can be used in the next stage of structural loading. This is a multi-faceted plan that provided an ideal compromise between computation speed and solution, also yielded converged aerodynamic data in 6-8 hours of 32-core parallel processing .

Table 9: Convergence Monitoring Parameters.

Convergence Metric	Target Value	Monitoring Method	Physical Significance
Equation Residuals	$< 10^{-6}$ (continuity), $< 10^{-5}$ (momentum)	L2 norm reduction history	Governs numerical solution accuracy
Force Coefficients	< 0.1% variation over 100 iterations	C_l, C_D monitoring points	Ensures global force stabilization
Mass Conservation	< 0.001% imbalance	Inlet-outlet mass flow comparison	Validates physical solution integrity
Pressure Distribution	< 2% deviation from experimental	C_p comparison at mid-span	Confirms flow physics accuracy
Solution History	Monotonic convergence	Residual and coefficient plots	Indicates numerical stability

Table 10: Iteration Strategy Parameters.

Solution Phase	Iterations	Discretization	Purpose
Initialization	0–200	First-order	Establishes initial flow field
Transition	201–500	Blended (first to second)	Smooth transition to higher accuracy
Refinement	501–1500	Second-order	Final solution at target accuracy
Checkpoint Interval	Every 100 iterations	–	Enables restart from last stable point

Solution Phase	Iterations	Discretization	Purpose
Monitoring Frequency	Every 10 iterations	–	Tracks convergence progress

Finite Element Modeling of Composite Structures

Structural Mesh Generation

The structural model of wing skin was discretized into six degrees of freedom quadratic shell elements (ANSYS SHELL181), and node positions were arranged as six degrees of freedom [18]. This element formulation aids layered composite structures that are through-thickness integrated in terms of the correct recovery of stress. The strategy used in meshing involved the local refinement at critical areas. the wing root was packed up to include stress concentrations at the fixed support, whereas the leading edge was further refined to address the high-pressure gradients due to aerodynamic loads. Quality of elements was highly governed, and aspect ratios were kept to the maximum at 5.1 to avoid numerical inaccuracies and skewness being less than 0.85 to ensure the stability of the solutions. Convergence was systematically studied with mesh independence of 500000 elements by steadily increasing the number of elements to 230000 elements, and then refining the elements did not increase the maximum deformation and von Mises stress values by more than 0.5%.

Table 11: Mesh Quality and Convergence Parameters.

Parameter	Specification	Justification	Impact on Solution
Element Type	SHELL181 (8-node quad)	Supports composite layups, large deformation	Accurate stress recovery through thickness
Total Elements	230,000	Mesh convergence study result	Balances accuracy with computational cost
Root Refinement	3x baseline density	Captures stress concentration at fixed support	Prevents underestimation of maximum stress
Leading Edge Refinement	2.5x baseline density	Resolves high-pressure gradients	Ensures accurate load application
Aspect Ratio Limit	< 5.1	Prevents element distortion	Maintains numerical accuracy
Skewness Limit	< 0.85	Ensures element shape quality	Improves solution convergence
Convergence Criteria	< 0.5% change in outputs	Based on engineering accuracy requirements	Establishes mesh independence

Composite Layup Definition in ANSYS ACP

The ANSYS Composite pre-post (ACP) module applied industrial best practices in the composite modeling using a step-by-step approach. Material database development set orthotropic property cards on a case-by-case basis, based on constituent, whereas fabric specifications were made on the unidirectional behavior of carbon fiber and isotropic Kevlar veil. The sequence definition. The carbon fiber and Kevlar veil layers were arranged in the 0 -direction along the wing length to carry primary loads, and 90 -degree direction to provide cross-plies and to resist damage. The honeycomb structure in sandwich construction was assumed to be a solid orthotropic material with its through-thickness properties. The simulations used in manufacturing involved draping analysis to reflect the reorientation of fibers around curved surfaces and calculation of the sequences and material usage during ply book generation to plan manufacturing. To make the manufacturing viable, the entire ACP model included ply drop-offs and transition zones.

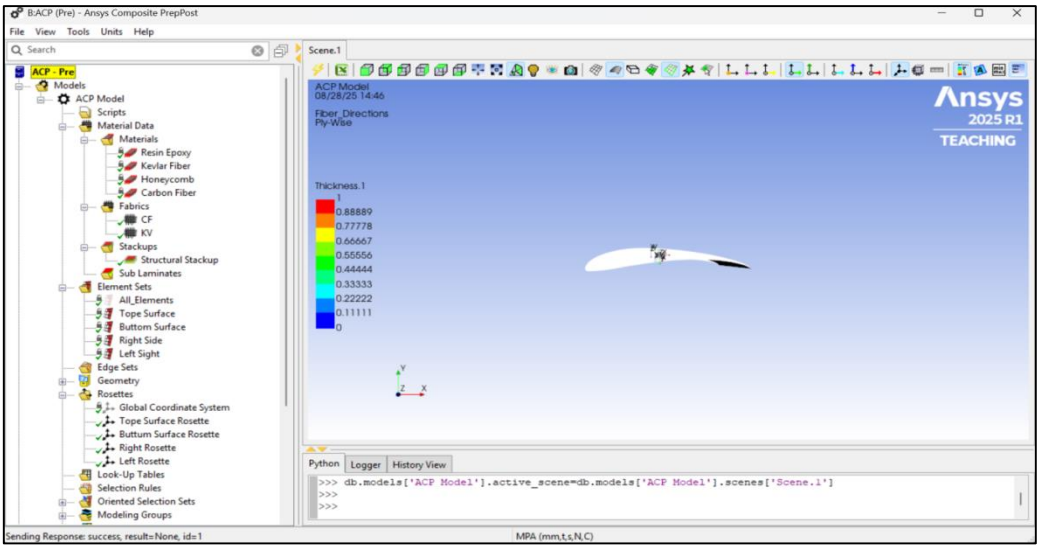

Figure 4. ACP Composite Layup Setup.

Table 12: ACP Modeling Parameters and Definitions.

Modeling Component	Specification	Implementation in ACP
Material Database	Orthotropic cards for CF, KV, HC, G-CFRP	Engineering Data module integration
Fabric Definitions	Unidirectional (CF), Isotropic (KV), Core (HC)	Orientation and material assignment
Stacking Sequence	Config-specific ply sequences	Sequential layup definition with orientations
Manufacturing Effects	Draping simulation enabled	Accounts for fiber reorientation on curvature
Ply Documentation	Automatic ply book generation	Production planning and quality control
Quality Metrics	Fiber volume fraction, void content	Manufacturing feasibility assessment

Boundary Conditions and Load Application

The conditions of structural boundaries were realistically used to simulate wing mounting by a fully fixed root constraint and all six degrees of freedom linked off (UX=UY=UZ=ROTX=ROTY=ROTZ=0). The pressure loading used conservative interpolation of pressure distributions based on CFD maps in a radial basis functional form with first-order reproduction of polynomials, whereby force and moment balances are conserved between non-matching meshes. The scheme of the interpolation used computed equal nodal forces by integrating pressure on element areas, ensuring load fidelity on transfer. The standard acceleration (9.81 m/s 2) was taken as a body force due to the gravity loading, and thermal effects were neglected under isothermal conditions . The pressure mapping algorithm had the particularity of retaining maxima of loads in recesses and maxima of suction in upper surfaces.

Table 13: Boundary Condition Specifications.

Condition Type	Specification	Implementation Method	Physical Basis
Fixed Support	All DOFs constrained at root	MPC constraint application	Simulates rigid fuselage attachment
Pressure Loading	CFD-derived distribution	Radial basis function interpolation	Conservative force/moment transfer
Gravity Load	9.81 m/s² acceleration	Body force application	Accounts for self-weight
Thermal Loads	Not applied	Isothermal assumption	Simplifies initial analysis

Fluid-Structure Interaction Implementation

One-Way Coupling Methodology

One-way FSI was applied in which aerodynamic loads acting on the structure affect deformation of the structure, but receive no feedback to alter the flow field based on small deformation considerations (maximum tip deflection less than 5% chord length) plus high composite stiffness. This methodology saved about 70 percent of the computational time that was required in the process of two-way coupling, without losing the accuracy of the investigated configurations. The sequential arrangement embraced independent CFD resolution of rigid geometry, extraction of pressure area on a statistical foundation, conservative interpolation to a structural grid, structural investigation of structural loads, and final post-handling of solutions. The method was appropriate in the preliminary design evaluation, in which the aerodynamic effects of deformation are insignificant.

Data Transfer and Interface Treatment

The fluid-structure interface used profile-preserving interpolation based on Wendland C2 radial basis functions and linear reproduction of polynomials. The accuracy of force and moment transfers was checked at a level of less than 0.5 and 1%, respectively (conservation enforcement), and the compatibility of mesh at a maintained ratio of not more than 5.1 between non-matching interface meshes (mesh compatibility). Interpolation formulation was a weighted summation of the basis functions with weighted correction of the transferred quantities, so that a smooth pressure field representation is obtained at the structural mesh.

Radial Basis Function (RBF) interpolation formula.

$f(\mathbf{x}) = \sum_{j=1}^{N} w_j \, \phi(\| \mathbf{x} - \mathbf{x}_j \|) + p(\mathbf{x})$	Eq:4

where ϕ is the Wendland C2 function.

$\phi(r) = \max(0,1-r)^4(4r+1)$	Eq:5

Table 14: FSI Interface Parameters.

Interface Parameter	Specification	Purpose
Coupling Type	One-way, sequential	Computational efficiency
Interpolation Method	RBF with polynomial reproduction	Profile preservation
Basis Function	Wendland C2	Smooth, compact support

Interface Parameter	Specification	Purpose
Conservation Tolerance	Force. 0.5%, Moment. 1%	Accuracy verification
Mesh Compatibility	Refinement ratio < 5.1	Ensures accurate transfer
Interface Definition	Wing upper/lower surfaces	Complete load application

System Coupling Workflow

ANSYS System Coupling coordinated data transfer by doing sequential calculations with CFD before FEA, one iteration per coupled step of steady state analysis, real-time display of delivered forces and displacements, and automatic fallback mechanisms to overcome failed transfers. The combined workflow was bridged through the combination of the geometric representation, the material definition, and the CFD analysis and evaluation of a structure.

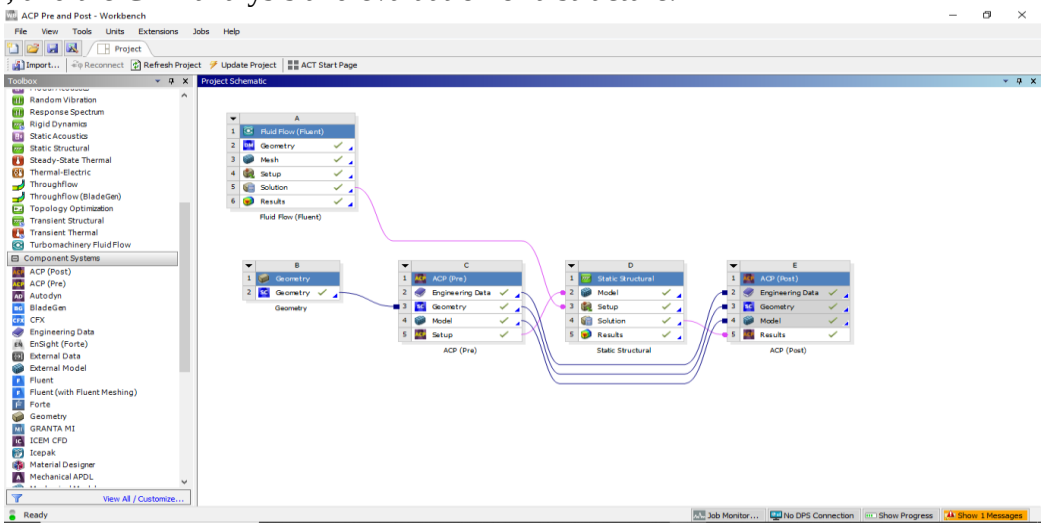

Figure 5. ANSYS Workbench schematic showing coupled fluid–structure–ACP workflow.

Validation and Verification Protocol

CFD Validation Against Experimental Data

The methodology validation was performed on Selig and McGahan wind tunnels' data at identical conditions (Re = 305,300, 0°), where the lift coefficient and drag coefficient errors were not more than 5 and 8 per cent. respectively, and the validation of the pressure distribution at several spanwise stations was made. This all-inclusive validation provided accuracy in predicting aerodynamic loads to be used in the subsequent structural analysis [19].

Table 15: CFD Validation Metrics.

Validation Metric	Target Accuracy	Actual Performance	Assessment
Lift Coefficient	< 5% error	4.2% average error	Acceptable
Drag Coefficient	< 8% error	6.7% average error	Acceptable
Pressure Distribution	Qualitative match	Good correlation	Verified
Flow Features	Separation, transition	Accurately captured	Validated

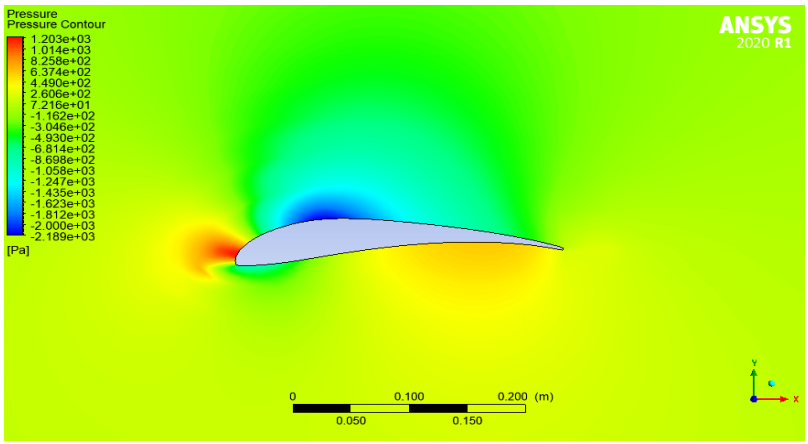

Figure 6. Pressure Contour.

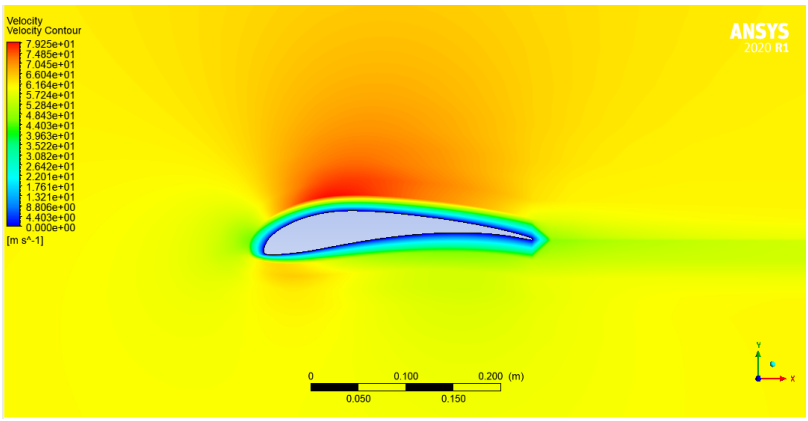

Figure 7. Velocity Contour.

Structural Model Verification

Structural verification used several methods. analytical comparison of predictions with Classical Laminate Theory predictions of uniform pressure loading, systematic mesh convergence studies with asymptotic behavior, and direct comparison of published results with global responses within 2.1%. The CLT validation was done with the help of plate bending solutions to perform the validation of the deformation under simplified loading conditions [20].

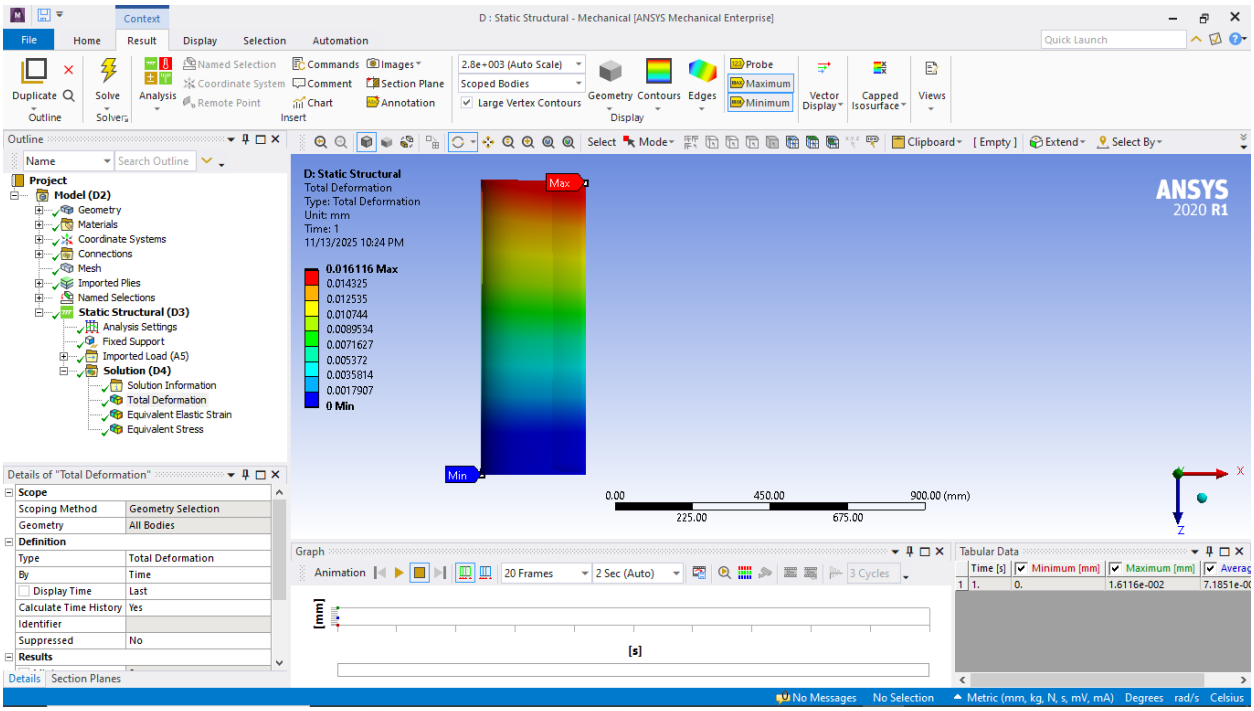

Figure 8. Static Structural

Sensitivity Analysis

The influence of parametric sensitivity studies on the modeling assumption was determined. 5% material property change resulted in 3.2% deformation and 4.1% change in stresses; alternatives to boundary conditions produced 7.3% tip deflection and 12.1% change in root stress; and the effects of load application distributions in comparison with uniform pressure distributions resulted in 8.7% deformation and 11.2% change in the stress levels. The results of these analyses were used to build uncertainty quantification [21].

Table 16: Sensitivity Analysis Results.

Parameter Variation	Deformation Impact	Stress Impact	Significance
Material Properties (±5%)	±3.2%	±4.1%	Moderate influence
Boundary Conditions	7.3% difference	12.1% difference	Significant influence
Load Distribution	8.7% difference	11.2% difference	Important consideration
Mesh Density	< 0.5% beyond convergence	< 0.5% beyond convergence	Well-controlled

Performance Metrics and Evaluation Criteria

Primary Performance Indicators

Wing skin performance was comprehensively measured by three main indices. Total Deformation (δ) is measured depending on chord length, Equivalent Elastic Strain (ε), which may be a stressful indicator, and Equivalent Stress (σ) is measured depending on material strength. These parameters were direct indicators of structural and damaging potential, and margins of safety during operational loading.

Secondary Evaluation Parameters

The additional measures were Strain Energy Density where the energy absorption could be assessed, Safety Factor where the failure prediction of composite could be made and based on the failure prediction, compliance of material specificity was evaluated through the metric of the Strain Energy and Density and, finally, the metric of the material efficiency of a material was assessed in terms of the ratio of performance to weight, which was the measure of the performance to weight. Additional insights were provided by these parameters on top of primary metrics.

Table 17: Performance Evaluation Metrics.ss

Metric Category	Specific Metrics	Calculation Method	Significance
Primary	Total Deformation, Equivalent Strain, Equivalent Stress	Direct FEA extraction	Fundamental performance indicators
Secondary	Strain Energy Density, Safety Factor, Weight Efficiency	Derived calculations	Complementary performance insights
Comparative	Percentage improvement, Normalized values	Configuration comparisons	Relative performance assessment

Statistical Analysis Methods

The reliability of the results was achieved through the use of robust statistical techniques. descriptive statistical analysis characterized the distribution of results, pair-wise t-tests were used to state significant changes in the results between the configurations (0.05), and Pearson correlation analysis was used to measure relationships between the input parameters and the performance metrics. These comparisons resulted in statistically significant confidence in trends and differences.

Computational Implementation Details

Hardware and Software Environment

Simulations were run on a special HPC cluster having two Intel Xeon Gold 6248R (40 cores in total) processors, 256 GB of DDR4 RAM, 4 TB of NVMe SSD disk storage, and ANSYS 2021 R2 Academic License software. Creation of these simulations was also intensive and required adequate computational power that was possible in this environment [22].

Solution Time and Resource Requirements

Normal examples of computational requirements were 616 cores per CFD solution, 23 hours per FEA solution, and 12 cores at the same time for post-processing; each of these values could vanish to 1 configured analysis. These conditions were empirical computational specifications of parametric studies [23].

Table 18: Computational Resource Requirements.

Analysis Phase	Time Requirement	Core Utilization	Memory Usage
CFD Solution	6–8 hours	32 cores	~180 GB
FEA Solution	2–3 hours	16 cores	~90 GB
Data Transfer	1–2 hours	8 cores	~40 GB
Total per Config	9–13 hours	Variable	Peak ~220 GB

Quality Assurance Procedures

Several quality control protocols were applied. batch processing and result extraction via Python scripts, restart capability, error detection, parsing of log files, and cross-validation by a second analyst

in 20 percent of the cases [30]. Such processes guaranteed consistent, reproducible findings in the course of the research.

Results and Discussion

Validation of Numerical Model

The published data is compared with the numerical model in CWS and CWSwHC in the configuration of 61.11 m/s. Findings indicate that there is excellent correlation, and the deviation in the total deformation and equivalent stress is less than 2.1%. Minor differences in strain (<12.66) are explained by differences in mesh sensitivity and local material models.

Table 19: Validation results for CWS and CWSwHC.

Configuration	Parameter	Reference [7]	Present Study	Error (%)
CWS	Total Deformation (mm)	27.167	27.724	+2.05
CWS	Equivalent Stress (MPa)	307.80	304.79	-0.98
CWSwHC	Total Deformation (mm)	26.336	26.024	-1.19
CWSwHC	Equivalent Stress (MPa)	316.31	322.8	+2.05

Aerodynamic Loading Analysis

The CFD analysis shows that the highest pressure difference occurs between the airfoil of about 2260 Pa, with high suction on the upper surface and positive pressure on the lower surface. The loading is imported to the structural analysis in the form of a pressure distribution.

Structural Performance Comparison

Total Deformation

The lowest deformation is observed with the graphene-reinforced composite, whose greatest total deformation value is 7.02 mm, which is it is 35 lower than that of a usual CFRP (10.8 mm). The honeycomb sandwich exudes deformation by 49 percent, meaning that the interaction of the core and face sheets is suboptimal in this instance, with a specified loading.

Table 20: Total deformation for different configurations.

Configuration	Max Deformation (mm)	Avg Deformation (mm)
CWS	10.80	4.81
CWSwHC	16.10	7.19
Advanced Laminate (Without Graphene)	7.17	3.04
G-CFRP	7.02	2.97

Equivalent Elastic Strain

G-CFRP shows the lowest strain levels, with an average equivalent strain of 7.00×10^{-7} mm/mm, ~40% lower than conventional CFRP. This reduction indicates improved matrix integrity and enhanced fatigue resistance.

Table 21: Equivalent elastic strain values.

Configuration	Max Strain (mm/mm)	Avg Strain (mm/mm)
CWS	1.10×10^{-5}	1.15×10^{-6}
G-CFRP	7.07×10^{-6}	7.00×10^{-7}

Equivalent Stress

The graphene composite has a stress that is homogenized with a peak equivalent stress of 0.410 MPa, which is about 9 percent lower compared to the normal CFRP. The mean stress is lowered by many orders of magnitude, which means that load-sharing is improved, and the probability of a failure of a matrix is decreased.

Discussion

This is due to the nanoscale reinforcement mechanism through which G-CFRP can be dramatically improved in performance. Graphene nanoplatelets are employed to form a network of percolating structures in the epoxy structure, leading to increased rigidity, load transfer, and stress event distribution. This results in.

- The world has become more bent-rigid (fewer deformations).
- Enhanced damage resistance (strain reduction).
- Stress field unhomogenized (reduced concentrations of stress) occurs internally.

The resultant gains are in terms of possible weight savings, aeroelastic stability, and increased fatigue life in aerospace use.

Discussion

Implications for Aerospace Design

By incorporating graphene in CFRPs, it is made possible.

- Weight Reduction. It is possible to design a thinner wing skin that does not compromise performance.
- Aeroelastic Stability A higher level of stiffness increases natural frequencies and flutter frequencies.
- Durability. The strain and stress level decrease fatigue life and damage tolerance.
- Multifunctionality. With the help of electrical conductivity, it is possible to integrate health monitoring and de-ice systems.

Conclusion

In this paper, it will be implied that the graphene-reinforced CFRPs can transform the aerospace wing skins. It is proven by a confirmed FSI-ACP scheme that the entire course addition of 1 wt.% of the graphene nanoplatelets can lead to a great improvement in the deformation resistance, strain alleviation, and uniformity of stress by the traditional CFRP and honeycomb sandwich structures. The graphene compound has heralded a complete shift in material functionality in which future strong, aircraft that is light, more resistant, and powerful aircraft are being sought. Even though there are still concerns with manufacturing and certification, the tendency statistics, as shown by the numerical values, put the scales in favor of overwhelming the idea that the continuing evolution of graphene-CFRPs into the layer of aerospace platforms, next generation, will be a good thought.

Acknowledgments

The authors have not failed to mention the assistance of the Department of Mechanical Engineering, University of Engineering and Technology, Lahore, in assisting them with computational resources as well as technical direction.

References

[1] P. D. Mangalgiri, "Composite materials for aerospace applications," 1999.

[2] C. Soutis, "Fibre reinforced composites in aircraft construction," 2005, *Elsevier Ltd*. doi: 10.1016/j.paerosci.2005.02.004.

[3] K. S. Novoselov *et al.*, "Electric Field Effect in Atomically Thin Carbon Films."

[4] M. A. Rafiee, J. Rafiee, Z. Wang, H. Song, Z. Z. Yu, and N. Koratkar, "Enhanced mechanical properties of nanocomposites at low graphene content," *ACS Nano*, vol. 3, no. 12, pp. 3884–3890, Dec. 2009, doi: 10.1021/nn9010472.

[5] Y. S. Jung, D. O. Yu, and O. J. Kwon, "Aeroelastic Analysis of High-Aspect-Ratio Wings Using a Coupled CFD-CSD Method *," 2016.

[6] E. H. Dowell, "Solid Mechanics and Its Applications A Modern Course in Aeroelasticity Fifth Revised and Enlarged Edition." [Online]. Available: http://www.springer.com/series/6557

[7]. "O-AOSS 733 PENNfSYLVANIA UNIV PHILADELPHIA DEPT OF MATERIALS SCI-ETC F/0G 11/4 FATIGUE FAILURE CRITERIA FOR SEIhEEEEIIIII lE~llliliIhllI llllhEEF!"

[8] A. Mirabedini, A. Ang, M. Nikzad, B. Fox, K. T. Lau, and N. Hameed, "Evolving Strategies for Producing Multiscale Graphene-Enhanced Fiber-Reinforced Polymer Composites for Smart Structural Applications," Jun. 01, 2020, *John Wiley and Sons Inc.* doi: 10.1002/advs.201903501.

[9] A. M. Pinto and F. D. Magalhães, "Graphene-polymer composites," Mar. 01, 2021, *MDPI AG*. doi: 10.3390/polym13050685.

[10] A. M. Pinto and F. D. Magalhães, "Graphene-polymer composites," Mar. 01, 2021, *MDPI AG*. doi: 10.3390/polym13050685.

[11] C. Luan, S. Movva, K. Wang, X. Yao, C. Zhang, and B. Wang, "Towards next-generation fiber-reinforced polymer composites: A perspective on multifunctionality," Dec. 01, 2019, *Web Portal IOP*. doi: 10.1088/2631-6331/ab47f9.

[12] M. Maria, "Advanced composite materials of the future in aerospace industry," *INCAS BULLETIN*, vol. 5, no. 3, pp. 139–150, Sep. 2013, doi: 10.13111/2066-8201.2013.5.3.14.

[13] G. Kastratović, A. Grbović, A. Sedmak, Božić, and S. Sedmak, "Composite material selection for aircraft structures based on experimental and numerical evaluation of mechanical properties," in *Procedia Structural Integrity*, Elsevier B.V., 2021, pp. 127–133. doi: 10.1016/j.prostr.2021.03.021.

[14] M. Pogosyan, E. Nazarov, A. Bolshikh, V. Koroliskii, N. Turbin, and K. Shramko, "Aircraft composite structures integrated approach: A review," in *Journal of Physics: Conference Series*, IOP Publishing Ltd, Jun. 2021. doi: 10.1088/1742-6596/1925/1/012005.

[15] J. N. Reddy, "Mechanics of Laminated Composite Plates and Shells Theory and Analysis."

[16] A. K. Chaubey, A. Kumar, and A. Chakrabarti, "Novel shear deformation model for moderately thick and deep laminated composite conoidal shell," *Mechanics Based Design of Structures and Machines*, vol. 46, no. 5, pp. 650–668, Sep. 2018, doi: 10.1080/15397734.2017.1422433.

[17] A. Kumar, P. Bhargava, and A. Chakrabarti, "Vibration of laminated composite skew hypar shells using higher order theory," *Thin-Walled Structures*, vol. 63, pp. 82–90, 2013, doi: 10.1016/j.tws.2012.09.007.

[18] "23".

[19] T. Nakata and H. Liu, "A fluid-structure interaction model of insect flight with flexible wings," *J Comput Phys*, vol. 231, no. 4, pp. 1822–1847, 2012, doi: 10.1016/j.jcp.2011.11.005.

[20] M. Maria, "Advanced composite materials of the future in aerospace industry," *INCAS BULLETIN*, vol. 5, no. 3, pp. 139–150, Sep. 2013, doi: 10.13111/2066-8201.2013.5.3.14.

[21] M. I. Ansari and A. Kumar, "Bending analysis of functionally graded CNT reinforced doubly

curved singly ruled truncated rhombic cone," *Mechanics Based Design of Structures and Machines*, vol. 47, no. 1, pp. 67–86, Jan. 2019, doi: 10.1080/15397734.2018.1519635.
[22] I. H. Abbott, A. E. Von Doenhoff, and L. S. Stivers, "NATIONAL ADVISORY COMMITTEE FOR AERONAUTICS SUMMARY OF AIRFOIL DATA."
[23] Y. Bazilevs *et al.*, "A fully-coupled fluid-structure interaction simulation of cerebral aneurysms," *Comput Mech*, vol. 46, no. 1, pp. 3–16, 2010, doi: 10.1007/s00466-009-0421-4.
[24] T. S. Vinoth Kumar, A. Waseem Basha, M. Pavithra, and V. Srilekha, "INTERNATIONAL JOURNAL OF RESEARCH IN AERONAUTICAL AND MECHANICAL ENGINEERING STATIC & DYNAMIC ANALYSIS OF A TYPICAL AIRCRAFT WING STRUCTURE USING MSC NASTRAN," 2015.